Aalto University

Albrecht, Elisabeth K.; Siponkoski, Tuomo; Rautama, Eeva-Leena; Karppinen, Maarit; Karttunen, Antti J.

Centrosymmetric to non-centrosymmetric transition in the $Ca_{2-x}Mn_xTi_2O_6$ double perovskite system studied through structural analysis and dielectric properties

Check for updates

Centrosymmetric to non-centrosymmetric transition in the $Ca_{2-x}Mn_xTi_2O_6$ double perovskite system studied through structural analysis and dielectric properties†

Elisabeth K. Albrecht,[a] Tuomo Siponkoski, [b] Eeva-Leena Rautama,[a] Maarit Karppinen [a] and Antti J. Karttunen [*a]

We have used high-pressure synthesis to synthesize samples of $Ca_{2-x}Mn_xTi_2O_6$ double perovskite, where x varies between 0.2 and 1. The synthesized materials were structurally characterized with powder X-ray diffraction (XRD). Rietveld refinement of the XRD patterns was used to study the change from $CaTiO_3$ ($x = 0$) to the composition $CaMnTi_2O_6$ ($x = 1$) where half of the Ca(II) ions are replaced by smaller Mn(II) ions. We analyzed the peak shapes in the XRD patterns, as well as lattice parameters, and it appears that smooth symmetry change from the centrosymmetric space group $Pbnm$ to the non-centrosymmetric space group $P4_2mc$ occurs between $x = 0.3$ and $x = 0.5$. We also confirmed the centrosymmetric to non-centrosymmetric transition by characterizing the dielectric properties of the materials with ferroelectric measurements.

1. Introduction

Ferroelectric materials show spontaneous polarization which is switchable by a sufficiently high electric field. When the polarization of a material is measured with respect to the applied electric field, ferroelectric materials show a hysteresis behaviour where the polarization does not reach zero when the electric field is switched off. The remaining polarization and the electric field needed to bring the polarization down to zero characterize the ferroelectric material. Especially for energy storage purposes, ferroelectrics are a promising option.[1,2] The storage of energy provided by renewable sources to guarantee on-demand energy supply is a pressing issue and ferroelectric materials could be used in the transformation towards a more sustainable energy infrastructure. Additionally, owing to their symmetry properties, ferroelectrics show by definition also pyroelectricity and piezoelectricity. Such materials have a whole set of interesting properties which can be tuned and optimized for different purposes such as sensors and energy harvesting.[3,4]

Perovskites are a wide class of compounds that are known for their various functionalities such as piezoelectricity, ferroelectricity, multiferroicity, superconductivity, and pyroelectricity.[5] The ideal perovskite structure has the composition ABX_3 with a cubic unit cell in the space group $Pm3m$. The X-anions form an octahedron around the B-cation, which sits in the center of the cube. The A-cation occupies the corners. While an ideal perovskite does not have a polar space group and thus cannot exhibit pyroelectricity, at room temperature perovskites often are distorted, the X-octahedra can be tilted and cations displaced.[6,7] The variety of properties is further increased when considering double perovskites, also called complex perovskites. In double perovskites, either the A-site or the B-site is occupied by two different elements, A-site (ordered) double perovskites ($AA'B_2X_6$) and B-site (ordered) double perovskites ($A_2BB'X_6$), respectively. While there has been a lot of research on B-site ordered double perovskites, A-site ordered double perovskites are much less researched. The cations can order in three different ways, columnar, planar or in a rock salt pattern.[8] The cations can also be disordered and form a solid solution.[9]

Unfortunately, the most common and efficient ferroelectric and thus pyroelectric (double) perovskites contain lead or bismuth which are toxic and harmful. The most well-known is $Pb(Zr,Ti)O_3$.[10] Lately, attention has been drawn to lead-free alternatives like $BaTiO_3$.[11–13] As for double perovskites, Aimi *et al.* used in 2014 high-pressure methods to synthesize a non-

[a]*Department of Chemistry and Materials Science, Aalto University, P.O. Box 16100, FI-00076 Aalto, Finland. E-mail: antti.karttunen@aalto.fi*
[b]*Microelectronics Research Unit, University of Oulu, P.O. Box 4500, FI-90014 Oulu, Finland*

†Electronic supplementary information (ESI) available: Additional *P–E* curves, lattice parameters of the studied materials, and Rietveld refinements of powder XRD patterns. See DOI: https://doi.org/10.1039/d4dt00360h

harmful A-site ordered double perovskite CaMnTi$_2$O$_6$ with a columnar cation ordering (see Fig. 1). Due to tilting of the oxygen octahedra, the A-site cation coordination deviates from the 12-fold coordination of an ideal perovskite. In the case of CaMnTi$_2$O$_6$, the Ca(II) cations are ten-fold coordinated, while half of the Mn(II) cations are tetrahedrally coordinated and the other half are square-planar coordinated. Aimi *et al.* also characterized the ferroelectric properties of the material, which arise from the displacement of the square-planar co-ordinated Mn(II) cations out of the plane.[14] In 2018, Li *et al.* proposed a new synthesis method for CaMnTi$_2$O$_6$, not using high pressure but spark plasma sintering. They also postulated a new mechanism for ferroelectricity in Ca$_{2-x}$Mn$_x$Ti$_2$O$_6$ ($x \leq$ 0.6).[15] Since its first synthesis, there has been more and more research on the material and its piezoelectric and ferroelectric properties.[16–19] Recently, we studied the proposed cation ordering and Glazer tilt system[20] of CaMnTi$_2$O$_6$ systematically with quantum chemical methods.[21]

Because CaMnTi$_2$O$_6$ is ferroelectric, it must also exhibit pyroelectric behaviour which has yet not been reported. To find the optimal composition range for the study of pyroelectricity, we investigate here the structural and ferroelectric behaviour of Ca$_{2-x}$Mn$_x$Ti$_2$O$_6$ with x = 0, 0.2, 0.3, 0.4, 0.5, 0.6, 0.7, 0.8 and 1. We aim to understand the phase transition from centrosymmetric space group *Pbnm* (x = 0) to the non-centrosymmetric space group *P4$_2$mc* (x = 1) and the connected change in the ferroelectric properties.
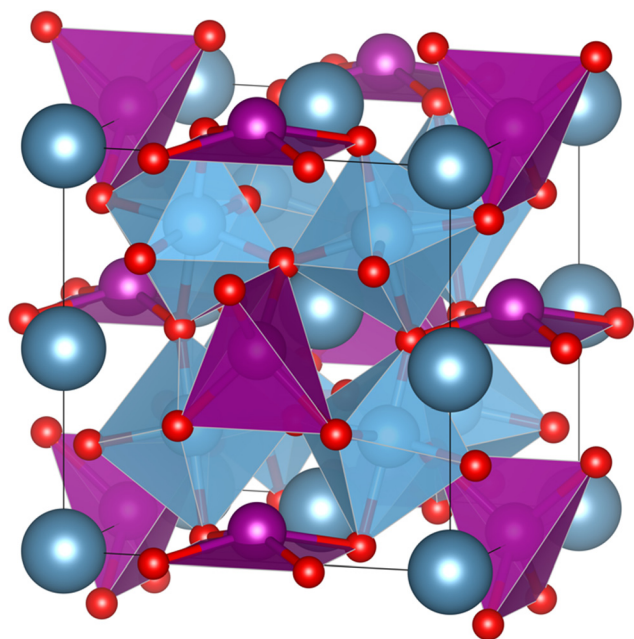

Fig. 1 Columnar A-site ordered double perovskite CaMnTi$_2$O$_6$ (*P4$_2$mc*).[14] Ca(II) cations are in dark grey-blue, Mn(II) cations and their coordination polyhedra in purple, Ti cations and their coordination polyhedra in blue and O anions in red. The crystal structure illustration has been prepared with the VESTA program.[22]

2. Experimental

X-ray diffraction measurements, as well as dielectric measurements were performed on Ca$_{2-x}$Mn$_x$Ti$_2$O$_6$ samples with $0 \leq x \leq 1$. Samples were prepared under high pressure and at high temperatures.

2.1. High-pressure synthesis

CaTiO$_3$ (Alfa Aesar, 99+% purity), MnO (Sigma Aldrich, 99% purity), and TiO$_2$ (Alfa Aesar, 99.5% purity) were used as precursors in a ratio according to x. The precursor powders were ground together in ethanol using an agate mortar and pestle. The dried powder mix was lightly pressed into a gold capsule. A cubic anvil geometry was used, for details on the high-pressure setup and sample preparation for the pressing, see ref. 23. The samples were synthesized at 4 GPa pressure. The synthesis temperature was limited by the melting point of the Au capsules at the given pressure, and therefore we aimed at a temperature right below the melting temperature. At temperatures of over 1000 °C, our calibration is not that accurate anymore, and the synthesis temperature of around 1250 °C is an estimate. The samples were held at the high pressure and temperature for 30 minutes, after which they were quenched to room temperature and the pressure was released.

2.2. Preparing samples for characterization

For the ferroelectric measurements, smaller discs were cut from the as-synthesized samples with a razor blade. To decrease the thickness of the samples further and to get a smooth and flat surface, the discs were ground with a sandpaper to a thickness between 0.23 mm and 0.55 mm. Disc diameters varied between 2.4 mm and 2.69 mm. In order to release the internal stress from the high pressure synthesis, the sample discs were annealed at 600 °C in oxygen atmosphere for 10 h. DuPot 5065 silver ink electrodes were painted on the discs and cured for 20 minutes between 110 and 120 °C. The part of each sample that was not used for making the discs was ground in an agate mortar to fine powder which was used for powder X-ray diffraction experiments.

2.2.1. Powder X-ray diffraction (XRD). Powder XRD measurements were performed by a PANalytical X'Pert Powder XRD with a Cu Kα$_1$ source. Rietveld refinements were done using the FullProf Suite.[24,25]

2.2.2. Ferroelectric measurements. Polarization (*P–E*) measurements were performed using a Radiant RT6000HVS ferroelectric tester. The measurement signal period was 50 ms (20 Hz) and the samples were measured at room temperature. Electric fields of up to 15 kV mm^{-1} (V μm^{-1}) were applied. The hysteresis loops were centered around the origin by adding an offset. The polarizations at zero electric field as well as the fields at zero polarization given here are the average of the absolute values of the positive and negative zero-field polarizations and zero-polarization fields, respectively.

2.2.3. Density measurements. For density determination, a sample of Ca$_{2-x}$Mn$_x$Ti$_2$O$_6$ with x = 0.5 was prepared and its volume measured by gas pycnometry using a Quantachrome

Ultrapyc 1200e. Afterwards, the sample was prepared for XRD measurement and the unit cell volume was determined by Le Bail fitting and Rietveld refinement.

3. Results and discussion

Samples of $Ca_{2-x}Mn_xTi_2O_6$ with $0 \leq x \leq 1$ were successfully synthesized, being close to phase pure. Some of the samples showed small (less than 2%) amounts of impurities (TiO_2, $MnTiO_3$, $CaCO_3$).

3.1. Structural analysis

For the series of compositions $Ca_{2-x}Mn_xTi_2O_6$ from $x = 0$ ($CaTiO_3$) to $x = 1$ ($CaMnTi_2O_6$), the unit cell volume was expected to decrease as a function of x since the Mn(II) ions gradually replacing the Ca(II) ions are significantly smaller compared to Ca(II) ions (the ionic radius of 12-coordinated Ca (II) is 1.34 Å, and the ionic radius of 4-coordinated Mn(II) is 0.66 Å[26]). The powder XRD patterns of all samples together with their Rietveld refinements are given in the ESI (Fig. S1–S8†). An explanation for the relatively large χ^2 values is the high pressure synthesis method and the internal strain induced by it. The lattice parameters obtained from the XRD analyses are also given in Table S1 of ESI.† Samples with $x = 0$ to 0.3 were refined in space group *Pbnm*, while samples with $x = 0.4$ to 1 could be refined in space group $P4_2mc$. The used space group was decided based on a comparison of each diffraction pattern with those of the end members of the series, $CaTiO_3$ ($x = 0$, *Pbnm*) and $CaMnTi_2O_6$ ($x = 1$, $P4_2mc$), which will be discussed later.

In order to compare unit cell volumes, the volume of the unit cells refined in *Pbnm* was scaled to fit the volume of unit cells refined in space group $P4_2mc$. The c lattice parameter is comparable in both space groups, *Pbnm* and $P4_2mc$, but the a and b parameter differ by a factor of about $\sqrt{2}$. Hence, a total scaling factor of 2 is applied to the volumes of the unit cells refined in *Pbnm* to match the volumes of the unit cells refined in $P4_2mc$. For $x = 0.3$ and $x = 0.4$, the Rietveld refinement was carried out in both space groups as parallel refinements. The double unit cell volume for $x = 0.3$ refined in *Pbnm* is 443.18 Å^3 and the volume in $P4_2mc$ is very close to it with a value of 443.29 Å^3. For $x = 0.4$, the volumes are 442.39 Å^3 and 442.53 Å^3 for space groups *Pbnm* and $P4_2mc$, respectively. However, a closer look at the powder X-ray diffraction patterns clearly showed the sample with $x = 0.3$ to adopt the orthorhombic crystal structure while the sample with $x = 0.4$ shows features of a tetragonal crystal structure. Fig. S9 in the ESI† shows an example for 2θ around 47.6° where the transition becomes visible. Fig. S10 in ESI† indicates how the ordering in the samples starts at $x = 0.4$, where a peak around $2\theta = 28.5°$ starts to appear. It is an example of a peak related to A-site cation ordering in space group $P4_2mc$.

Fig. 2 shows the resulting relation between the unit cell volume and the increasing amount of Mn(II) substitution described by x in $Ca_{2-x}Mn_xTi_2O_6$. With an increasing amount
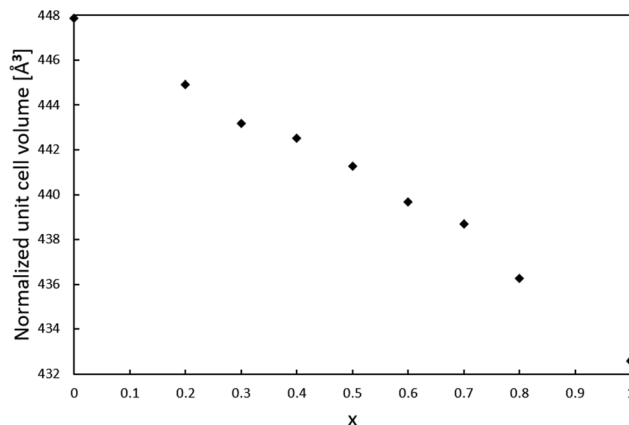

Fig. 2 Relation between the unit cell volume and the amount x of Mn(II) substitution in $Ca_{2-x}Mn_xTi_2O_6$. The unit cell volume of phases refined in space group *Pbnm* has been scaled with a factor 2 to fit the volume of unit cells refined in $P4_2mc$.

of Mn(II), the unit cell volume becomes smaller, as expected from the smaller Mn(II) ions replacing the larger Ca(II) ions.

Since the lattice parameter c spans over two oxygen octahedra in both space groups *Pbnm* and $P4_2mc$, its behavior as a function of x was expected to resemble the behaviour of the unit cell volume. Interestingly, the c lattice parameter was not found to strictly shrink with respect to x. As shown in Fig. 3, the length of the c-parameter decreases as expected in general when moving from $x = 0$ to $x = 1$ but suddenly increases between $x = 0.3$ and $x = 0.5$, after which the parameter decreases again as expected. No evidence was found in the XRD patterns for a mixed phase of $CaTiO_3$ and $CaMnTi_2O_6$ being responsible for the behavior of the c-lattice parameter. The range in which the lattice parameter deviates from the expected behavior indicates the phase transition and is probably connected to the appearance of polarization along the c-axis. As a comparison, Fig. S11 in the ESI† shows the change of the a and b lattice parameters with respect to x. The change
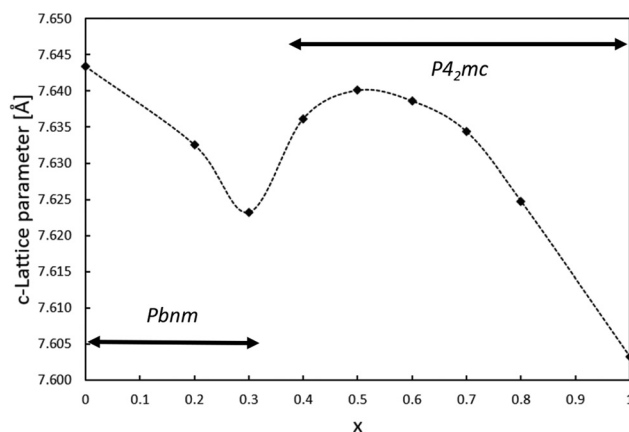

Fig. 3 Relation between the lattice parameter c and the amount of Mn (II) substitution in $Ca_{2-x}Mn_xTi_2O_6$.

could also be observed from the changes seen in the diffraction patterns (Fig. S2 and S3 in the ESI†). Li *et al.*[15] found the intensity of the second harmonic generation to be close to the background for $x < 0.3$[15] which indicates the loss of non-centrosymmetry and therefore polarity in the unit cell. This is in line with our observations on the phase transition. Even in the overall unit cell volume in Fig. 2, a slight irregularity is observed around $x = 0.4$. As discussed above, samples of $x = 0.3$ and $x = 0.4$ were refined in both space groups *Pbnm* and *P4$_2$mc*. The *c*-parameters of $x = 0.3$ are 7.623 Å and 7.628 Å, respectively and for $x = 0.4$ they are 7.635 Å and 7.636 Å, respectively. Even though the difference in space group results in larger differences in the *c* lattice parameter compared to unit cell volume, still the overall trend of the series remains the same.

The phase transition is evident in the change of the main peak area in the powder diffraction patterns, around $2\theta = 33°$ (Fig. 4). When x changes from 0 to 1, the position of the main peak shifts only slightly due to the change in lattice parameters but the two neighboring peaks in CaTiO$_3$ first vanish and then the side peak of CaMnTi$_2$O$_6$ emerges. With the unit cell, also the Miller indices of the peak change from (112) in CaTiO$_3$ (*Pbnm*) to (202) in CaMnTi$_2$O$_6$ (*P4$_2$mc*). From Fig. 4 it is clear that the phase transition must occur between $x = 0.3$ and $x = 0.4$ where there are no distinct peaks visible. As discussed above, another example of a clear change in the XRD patterns indicating the phase transition is the appearance of the (112) and (121) peaks around $2\theta = 28.6°$ in the sample with $x = 0.4$ (Fig. S10 in the ESI†).

3.2. Density

The average density of an as-synthetized Ca$_{1.5}$Mn$_{0.5}$Ti$_2$O$_6$ sample from ten volume measurements is 4.09 g cm^{-3} which corresponds to a relative density of over 97%. The high density is to be expected for samples synthesized under high pressure and due to the robustness of the synthesis method we assume all samples in the studied series to have a similarly high density. The density measurement provides no information of possible pores in the sample since the gas of the pyctometric measurement penetrates into these.

3.3. Ferroelectric analysis

The samples in general were rather unstable under electric field and had a tendency to break down during measurements before saturation was reached. An explanation of the weak resistance against breakdowns can be found in the synthetic approach. Even though the samples have been heat treated afterwards, there is a possibility of remaining stress due to the high pressure during the synthesis process. Additionally, the samples are rather brittle which makes them even more susceptible towards a breakdown in medium to high electric fields. In those cases where the sample was able to withstand higher electric fields, saturation in the hysteresis polarization curve was not reached because of the sample thickness and the maximum voltage of the measurement setup was limited to 4 kV. Samples were too brittle to be prepared thinner in order to achieve higher fields. The numbers mentioned in the following discussion are for the purpose of comparison and neither the true remanent polarization nor the true coercive field.
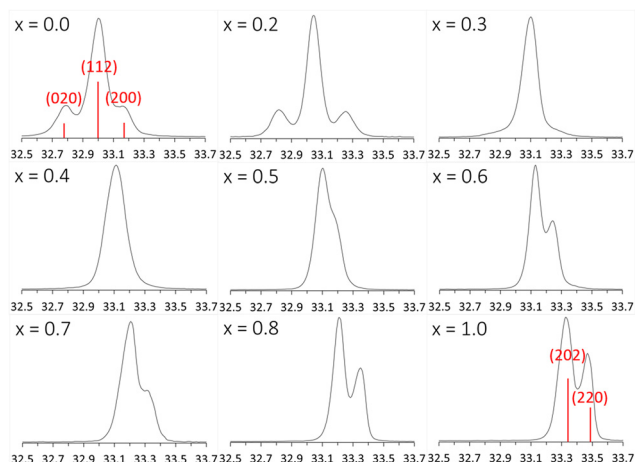

Fig. 4 Changes in the main peak area, around $2\theta = 33°$ in the powder diffraction pattern of Ca$_{2-x}$Mn$_x$Ti$_2$O$_6$ from CaTiO$_3$ ($x = 0$) to CaMnTi$_2$O$_6$ ($x = 1$). The Miller indices of the main peak of $x = 0$ (*Pbnm*) are (112) and the ones on the side (020) and (200), depending on the orientation. For $x = 1$ (*P4$_2$mc*), the main peaks are (202) and (220).
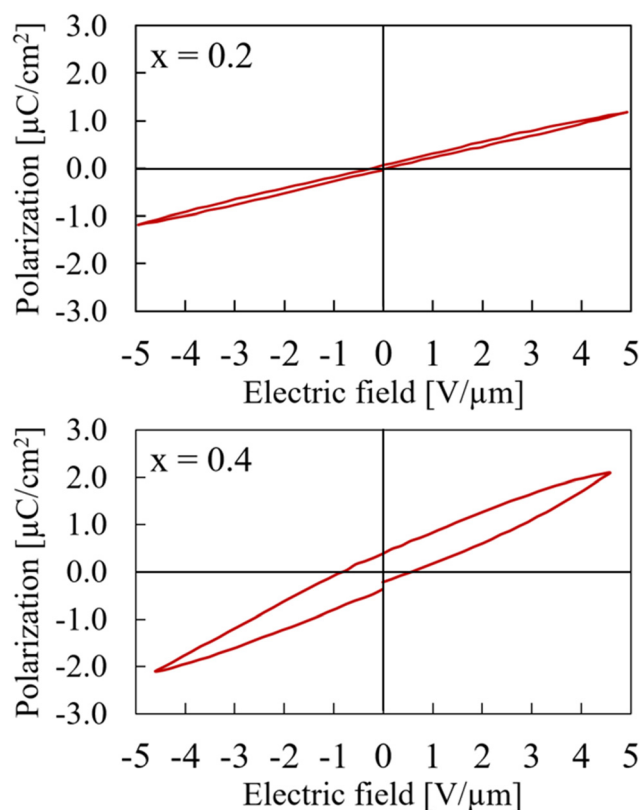

Fig. 5 Hysteresis curves of Ca$_{2-x}$Mn$_x$Ti$_2$O$_6$ with $x = 0.2$ (upper) and $x = 0.4$ (lower) at maximum electric field of 5 V μm^{-1}.

As expected from the structural data, the sample with x = 0.2 basically shows linear behavior in a P–E measurement. Since the sample still adopts the centrosymmetric structure of $CaTiO_3$, no remanent polarisation can be measured. The sample with x = 0.4, which was refined in the non-centrosymmetric space group $P4_2mc$ still exhibits more or less linear behaviour but with a slight hysteresis starts to emerge. This, again, indicates a smooth structural transition around this composition rather than a sudden switch between space groups $Pbnm$ and $P4_2mc$. Both P–E measurements for x = 0.2 and x = 0.4 are shown in Fig. 5. For comparison, they are both shown with a maximum field of about 5 V μm^{-1}. The hysteresis curve of the x = 0.4 sample with a maximum field of 15 V μm^{-1} is available in ESI as Fig. S12.†

Samples with x between 0.5 and 1 adopt the non-centrosymmetric $CaMnTi_2O_6$ structure based on the XRD analysis and therefore a ferroelectric hysteresis loop should be detected. However, this is only the case for x = 0.5 and x = 0.6. The hysteresis curves are shown in Fig. 6. The measurement with x = 0.6 has a higher zero-field polarization P_r = 3.11 µC cm^{-2} as well as a higher zero-polarization field E_c = 4.78 V μm^{-1}. P_r for the sample with x = 0.5 is determined to be only 1.62 µC cm^{-2} and E_c = 3.17 V μm^{-1}. Because the sample x = 0.6 had a breakdown after 12 V μm^{-1}, the comparison in Fig. 6 is shown for a maximum field of 12 V μm^{-1}, even though it

was possible to measure the x = 0.5 sample up to the device limit of 15 V μm^{-1}.

Interestingly, the polarization measurements of the samples with x = 0.7, x = 0.8, and x = 1.0 all display large leakage currents and respond like a highly leaking capacitor (slight linearity in polarization).(Fig. 7). Especially for the x = 1.0 sample, which is pure $CaMnTi_2O_6$, the result differs from literature reports where ferroelectric hysteresis loops for fields up to 20 V μm^{-1} were measured.[14] However, our samples with x = 1.0 always contained at least a small amount of single crystals which were loosely packed together with the bulk material. The sample seemed more crumbly than those with smaller x. The single crystals were detected amongst the regular powder
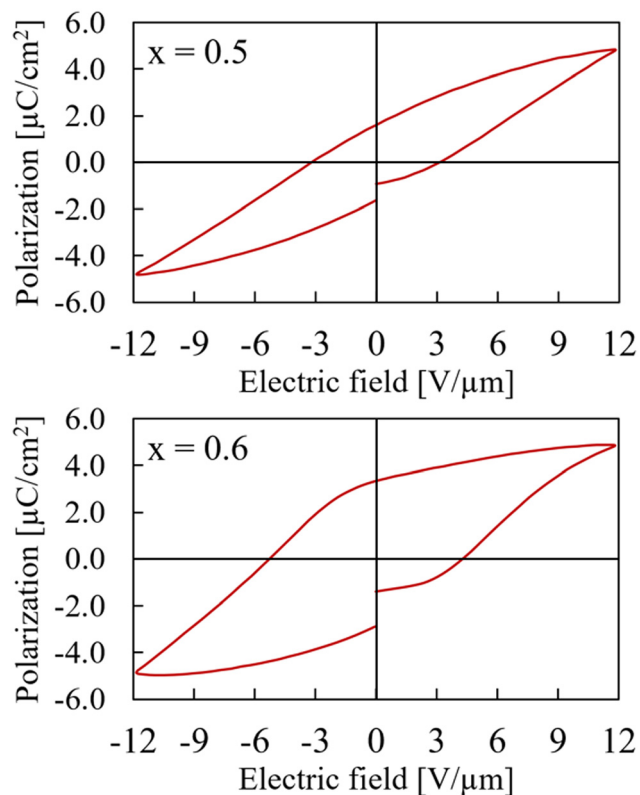

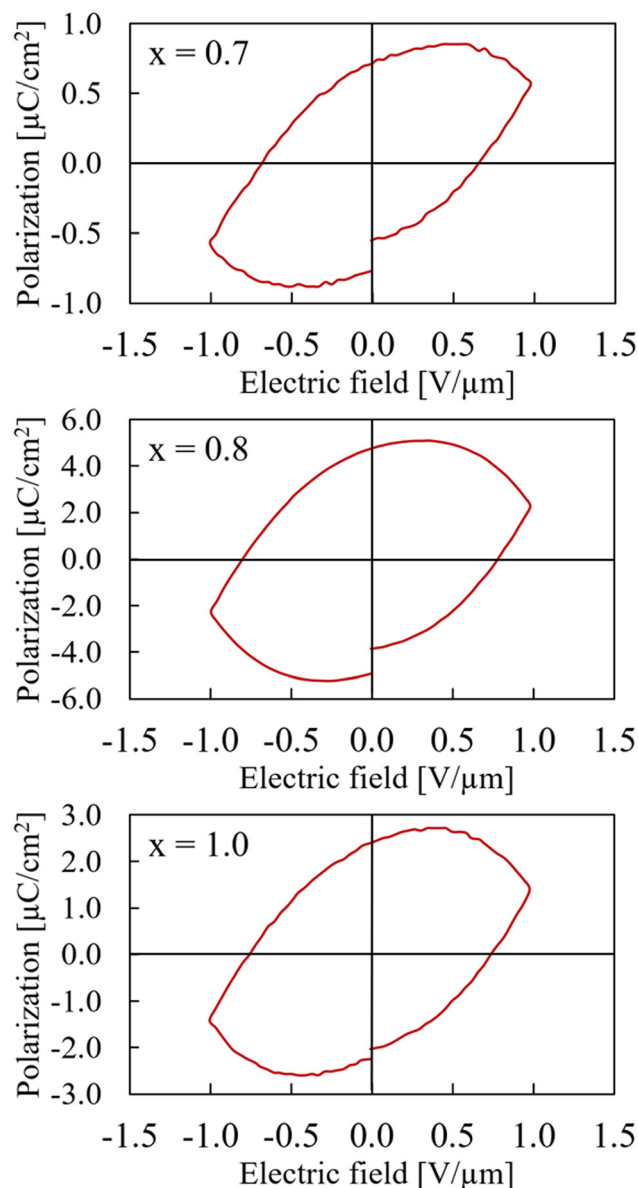**Fig. 7** Hysteresis curves of $Ca_{2-x}Mn_xTi_2O_6$ with x = 0.7 (upper), x = 0.8 (middle), and x = 1.0 (lower) at maximum electric field of 1 V μm^{-1}. Note that the polarization axes have different scales.

Fig. 6 Hysteresis curves of $Ca_{2-x}Mn_xTi_2O_6$ with x = 0.5 (upper) and x = 0.6 (lower) at maximum electric field of 12 V μm^{-1}.

particles after grinding the sample as preparation for XRD measurements. Aimi *et al.* do not report any single crystals in the samples used for polarization measurements. While the pressed bulk sample has a high relative density, the connection of single crystals to the bulk is rather loose. This leads to resistor-like behaviour. However, the $x = 1.0$ sample showed a mixture of hysteresis and resistor-like behaviour at smaller maximum fields (Fig. S13 in ESI†).

4. Conclusions

We have synthesized samples of $Ca_{2-x}Mn_xTi_2O_6$ with $x = 0.2$; 0.3; 0.4; 0.5; 0.6; 0.7; 0.8; and 1.0. A structural analysis of these samples identified the phase transition between the centrosymmetric space group *Pbnm* of $x = 0$ ($CaTiO_3$) and the non-centrosymmetric space group $P4_2mc$ of $x = 1$ ($CaMnTi_2O_6$) to be around $x = 0.4$. This has been shown in the change of the XRD pattern around the main peak at a 2θ of about 33° and the non-linear change in the c lattice parameter. While the lattice parameters are expected to shrink from $x = 0$ to $x = 1$ due to substitution of the larger Ca(II) ions by the smaller Mn(II) ions, the c lattice parameter increases between $x = 0.3$ and $x = 0.5$. *P–E* measurements also confirmed a linear behaviour for $x = 0.2$ and a clear hysteresis and therefore ferroelectricity for $x = 0.5$ and 0.6. However, for $x = 0.7$ and higher, no hysteresis was measured but rather resistor-like behaviour. With our synthesis and characterization methods, a composition of $Ca_{2-x}Mn_xTi_2O_6$ with $x = 0.6$ appears to lead to the strongest ferroelectricity. However, it can be expected that the zero-field polarization and the zero-polarization field further increase in samples of $x = 0.7$ to 1.0. Therefore, no final conclusion can be made about the optimal composition of $Ca_{2-x}Mn_xTi_2O_6$ for ferroelectric purposes. The samples with $x > 0.7$ behave like resistor and do not show their whole ferroelectric and therefore pyroelectric potential due to a poor coupling between formed single crystals and the bulk sample. It was not possible to completely avoid the formation of single crystals during the synthesis of samples with large x. A detailed investigation on the formed single crystals will be provided elsewhere.

Author contributions

Elisabeth K. Albrecht: Conceptualization; investigation; visualization; writing – original draft preparation; writing – review and editing. Tuomo Siponkoski: Investigation (ferroelectric measurements); writing – review and editing. Eeva-Leena Rautama: Investigation (Rietveld refinement); writing – review and editing. Maarit Karppinen: Resources; writing – review and editing. Antti J. Karttunen: Conceptualization; writing – review and editing; supervision; funding acquisition. All authors have read and agreed to the published version of the manuscript.

Conflicts of interest

There are no conflicts to declare.

Acknowledgements

References

1 V. Veerapandiyan, F. Benes, T. Gindel and M. Deluca, *Materials*, 2020, **13**, 5742.
2 P. Gao, Z. Liu, N. Zhang, H. Wu, A. A. Bokov, W. Ren and Z.-G. Ye, *Chem. Mater.*, 2019, **31**, 979–990.
3 J. F. Nye, *Physical properties of solids*, Oxford University Press, 1957.
4 K. M. Ok, E. O. Chi and P. S. Halasyamani, *Chem. Soc. Rev.*, 2006, **35**, 710.
5 R. J. D. Tilley, *Perovskites: structure-property relationships*, Wiley, Chichester, West Sussex, United Kingdom, 1st edn, 2016.
6 P. M. Woodward, *Acta Crystallogr., Sect. B: Struct. Sci.*, 1997, **53**, 32–43.
7 P. M. Woodward, *Acta Crystallogr., Sect. B: Struct. Sci.*, 1997, **53**, 44–66.
8 G. King and P. M. Woodward, *J. Mater. Chem.*, 2010, **20**, 5785.
9 A. Bokov, N. Protsenko and Z.-G. Ye, *J. Phys. Chem. Solids*, 2000, **61**, 1519–1527.
10 B. Jaffe, W. R. Cook and H. L. Jaffe, *Piezoelectric ceramics*, Academic Press, London, New York, 1971.
11 S. Zhang, R. Xia and T. R. Shrout, *J. Electroceram.*, 2007, **19**, 251–257.
12 T. R. Shrout and S. J. Zhang, *J. Electroceram.*, 2007, **19**, 113–126.
13 J. Jia, S. Guo, S. Yan, F. Cao, C. Yao, X. Dong and G. Wang, *Appl. Phys. Lett.*, 2019, **114**, 032902.
14 A. Aimi, D. Mori, K.-I. Hiraki, T. Takahashi, Y. J. Shan, Y. Shirako, J. Zhou and Y. Inaguma, *Chem. Mater.*, 2014, **26**, 2601–2608.
15 Z. Li, Y. Cho, X. Li, X. Li, A. Aimi, Y. Inaguma, J. A. Alonso, M. T. Fernandez-Diaz, J. Yan, M. C. Downer, G. Henkelman, J. B. Goodenough and J. Zhou, *J. Am. Chem. Soc.*, 2018, **140**, 2214–2220.

16 J. Ruiz-Fuertes, T. Bernert, D. Zimmer, N. Schrodt, M. Koch-Müller, B. Winkler, L. Bayarjargal, C. Popescu, S. MacLeod and K. Glazyrin, *Phys. Rev. B*, 2017, **96**, 094101.

17 G. Gou, N. Charles, J. Shi and J. M. Rondinelli, *Inorg. Chem.*, 2017, **56**, 11854–11861.

18 J. Herrero-Martín, J. Ruiz-Fuertes, T. Bernert, M. Koch-Müller, E. Haussühl and J. L. García-Muñoz, *Phys. Rev. B*, 2018, **97**, 235129.

19 R. A. Maier, K. F. Garrity, A. Ozarowski, M. P. Donohue, G. Cibin and I. Levin, *Acta Mater.*, 2021, **207**, 116688.

20 A. M. Glazer, *Acta Crystallogr., Sect. B: Struct. Crystallogr. Cryst. Chem.*, 1972, **28**, 3384–3392.

21 E. K. Albrecht and A. J. Karttunen, *Dalton Trans.*, 2022, **51**, 16508–16516.

22 K. Momma and F. Izumi, *J. Appl. Crystallogr.*, 2011, **44**, 1272–1276.

23 L. Sederholm, T. Tiittanen and M. Karppinen, *J. Solid State Chem.*, 2023, **317**, 123646.

24 J. Rodríguez-Carvajal, *Phys. B*, 1993, **192**, 55–69.

25 T. Roisnel and J. Rodriguez-Carvajal, Proceedings of the Seventh European Powder Diffraction Conference (EPDIC 7), 2000, pp. 118–123.

26 R. D. Shannon, *Acta Crystallogr., Sect. A: Cryst. Phys., Diffr., Theor. Gen. Crystallogr.*, 1976, **32**, 751–767.